RESEARCH ARTICLE

Four-step spin crossover in a new cyano-bridged iron-silver coordination polymer

Olesia I. Kucheriv,[a] Sergii I. Shylin,[b,c] Valerii Y. Sirenko,[a] Vadim Ksenofontov,[b] Wolfgang Tremel,[b] Ioan-Andrei Dascălu,[d] Sergiu Shova,[d] and Il'ya A. Gural'skiy*[a]

[a] O.I. Kucheriv, V.Y. Sirenko, Dr. I.A. Gural'skiy
Department of Chemistry
Taras Shevchenko National University of Kyiv
Volodymyrska St. 64, Kyiv 01601 (Ukraine)
E-mail: illia.guralskyi@univ.kiev.ua

[b] Dr. S.I. Shylin, Dr. V. Ksenofontov, Prof. W. Tremel
Institute of Inorganic and Analytical Chemistry
Johannes Gutenberg University of Mainz
Staudingerweg 9, Mainz 55099 (Germany)

[c] Dr. S.I. Shylin
Department of Chemistry – Ångström Laboratory
Uppsala University
Uppsala 75120 (Sweden)

[d] Dr. I.-A. Dascălu, Dr. S. Shova
Department of Inorganic Polymers
Institute of Macromolecular Chemistry "Petru Poni"
Aleea Grigore Ghica Voda 41A, Iasi 700487 (Romania)

Supporting information for this article is given via a link at the end of the document.

Abstract: Spin-crossover complexes with multistep transitions attract much attention due to their potential applications as multi-switches and for data storage. A four-step spin crossover is observed in the new iron(II)-based cyanometallic guest-free framework compound $Fe(2\text{-ethoxy-pyrazine})_2\{Ag(CN)_2\}_2$ during the transition from the low-spin to the high-spin state. A reverse process occurs in three steps. Crystallographic studies reveal an associated stepwise evolution of the crystal structures. Multiple transitions in the reported complex originate from distinct Fe^{II} sites which exist due to the packing of the ligand with a bulky substituent.

Introduction

Phase-transition solids attract attention as materials for data storage,[1] construction of actuators,[2] electronic components,[3] etc. Spin transition complexes are the most common class of molecular switches. $3d^4$-$3d^7$ metal cations can exist in different electronic configurations, the so-called high-spin (HS) and low-spin (LS) states. This leads to a large class of spin-crossover (SCO) compounds that can switch between HS and LS states by external stimuli.[4] Different applications of pure and hybrid SCO materials are envisaged, for example, for electronics,[5] actuation,[6] sensor technology.[7]

Cyanometallates with square-planar and octahedrally coordinated metal ions have been known since 1903 for their ability to incorporate various organic and inorganic molecules.[8] Their structure contains layers of M^{2+} cations linked by $M'(CN)_4$ units with axial co-ligands coordinated to octahedral centers, which connect these layers into a rigid two- or three-dimensional framework. The iron(II) based analogue $[Fe(py)_2Ni(CN)_4]$ was found to exhibit SCO behavior previously.[9] This prompted synthetic activities to make new analogues of Hofmann clathrates with SCO, which are now one of the biggest families of SCO complexes.[10] Besides cyanometallates with square-planar coordination, other units, especially linear $M(CN)_2^-$ (M = Cu, Ag, Au) units, are highly useful for building up such SCO frameworks.[11]

Multistep spin transitions are characterized by the existence of individual states with different functional characteristics. They show multiple regimes of switching. When the SCO is hysteretic, it can have several memory channels. Complexes with multistage transitions have one of the following characteristics: (1) crystallographically distinct Fe^{II} centers undergoing a SCO at different temperatures, (2) the reduction of symmetry in an intermediate state where previously equivalent Fe^{II} centers become non-equivalent, (3) the formation of mixed centers when HS and LS states coexist. These mechanisms or their combination allow to achieve transitions with two, three, four and even more steps.[12]

Two-step transitions are the most common among all the types of multistep SCO in complexes. Three- and more step transitions are much less widespread and the mechanisms of such transitions remain not fully explored. Such multistep transitions are usually realized through cooperative lattice effects which favor stabilization of Fe^{II} centers with different spin states. Complexes with three- and more step transitions usually feature more complicated geometries of crystal lattice which can result in the formation of crystallographically inequivalent Fe^{II} sites and/or provide the possibility for symmetry breaking. Most often complexes which undergo SCO in multiple steps contain guest molecules, which provide a set of antagonistic host–guest, host–host or guest–guest interactions that contribute to the necessary asymmetry of the structure. Thus, relative flexibility of 2D cyanometallic layers in combination with a set of weak interactions allows to achieve complex multistep schemes of spin state variation with temperature. More information concerning the mechanisms of multistep transitions can be found in ref. [13].

The first SCO system exhibiting four-step SCO was offered by Kepert et al. in 2016.[12a] This was a Hofmann clathrate analogue $[Fe^{II}(bipydz)\{Au^{I}(CN)_2\}_2]\cdot 4(EtOH)$ (bipydz = 3,6-bis(4-pyridyl)-1,2-diazine) which displayed the sequence of transformations HS → $HS_{0.67}LS_{0.33}$ → $HS_{0.5}LS_{0.5}$ →$HS_{0.33}LS_{0.67}$ →LS. Since then there were several reports on other SCO complexes which undergo multistep transitions,[14] including one exceptional example of a complex with seven/eight-step transition obtained by Tong et al. in 2020.[15]

Here we describe the complex $[Fe(EtOpz)_2\{Ag(CN)_2\}_2]$ (**1**, EtOpz = 2-ethoxypyrazine) whose structure contains layers of Fe^{2+} cations linked by $Ag(CN)_2^-$ groups that are supported by 2-substituted pyrazine molecules which provides a rare example of a four-step SCO in a guest free framework. Similar pyrazine derivatives are known to form SCO complexes.[16]

Results and Discussion

The magnetic behavior of **1** as a function of temperature is shown in **Figure 1** (its derivative shown in **Figure S1**). At low temperature (below 120 K) **1** is diamagnetic with a residual $\chi_M T$ of 0.22 $cm^3\,mol^{-1}\,K$. Upon heating all iron(II) centers switch to the HS state ($\chi_M T$ = 3.33 $cm^3\,mol^{-1}\,K$ at 280 K). This transformation proceeds in four steps. The first step is hysteretic with $T_c^{up}(1)$ = 133 K and $T_c^{down}(1)$ = 127 K. Only 1/3 of all iron centers undergo a transformation at this step ($\chi_M T$ = 1.10 $cm^3\,mol^{-1}\,K$ at 160 K).

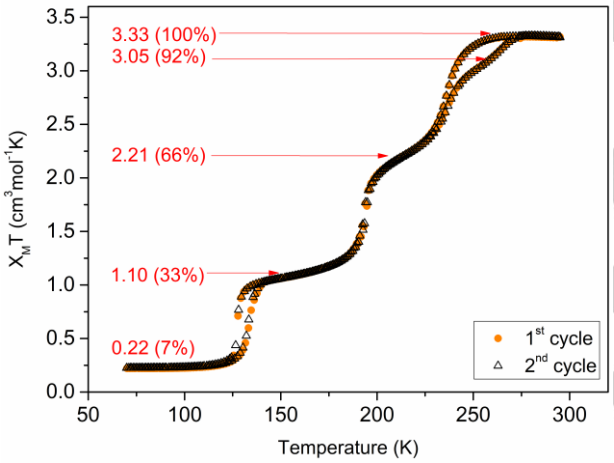

Figure 1. Magnetic properties of **1** measured in two consequent cycles. A four-step SCO is observed during the LS to HS transition upon heating, whereas the back process has a three-step character. The $\chi_M T$ values for each plateau are provided in absolute values and in percent of the HS $\chi_M T$ value.

The second step also involves only 1/3 of Fe centers. It is non-hysteretic with a transition temperature $T_c(2)$ = 194 K. The remaining 1/3 of the iron centers transform in steps 3 and 4. Upon cooling, the corresponding conversion occurs in a single step (heating and cooling $T_c(3)$ = 236 K, with an additional step upon heating $T_c^{up}(4)$ = 265 K).

1 crystallizes in the centrosymmetric space group $P2_1/c$. The crystal structure contains three independent Fe sites (**Figure 2a**). All of them contain octahedral FeN_6 units with four $Ag(CN)_2$ moieties in the equatorial (in plane) and two ethoxypyrazine molecules in the axial (out of plane) positions. At 115 K, all iron centers are in the LS state. This is evident from the Fe-N bond

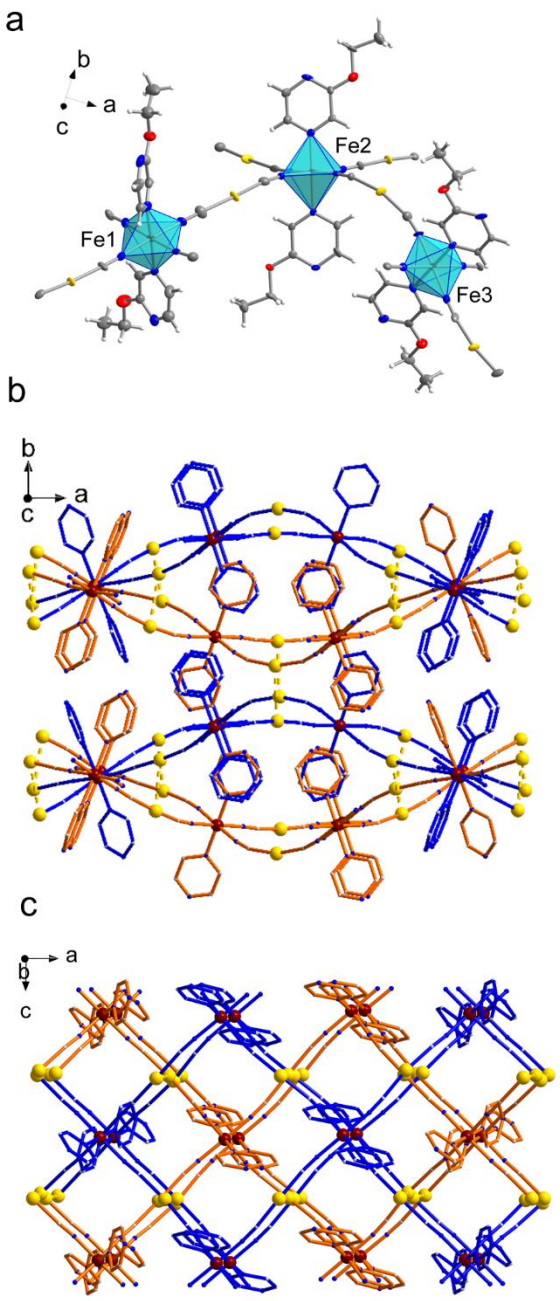

Figure 2. (a) Fragment of the crystal structure of **1** (115 K) showing three iron centers in N6 coordination environment displaying thermal SCO. H atoms are omitted. Color code: Fe red, Ag yellow, C grey, N blue, O red. Thermal ellipsoids are drawn at 50% probability. (b) The structure of framework **1** showing the interaction between cyanometallic grids. (c) A projection of the structure **1** in *ac* plane showing (4,4) network topology. In figures b and c H atoms and ethoxy groups are omitted for clarity.

lengths. For Fe1, the Fe-N_{CN} bond lengths are 1.95-1.98 Å and the Fe-N_{pz} bond lengths are 1.97-2.04 Å. For Fe2 the Fe-N_{CN} bond lengths are 1.94-1.96 Å and the Fe-N_{pz} lengths are 2.00 Å. For Fe3 the Fe-N_{CN} bond lengths are 1.94-1.96 Å and the Fe-N_{pz} lengths are 1.98-1.99 Å. The average values are compiled in **Table 1**. At the first step of the spin transition the Fe2 and Fe3

Table 1. Selected crystallographic information for **1** at five different temperatures.

T(K)	a (Å)	b (Å)	c (Å)	β (°)	V (Å)	Fe1-$N_{av.}$ (Å)	Fe2-$N_{av.}$ (Å)	Fe3-$N_{av.}$ (Å)	Ag1--Ag2 (Å)	Ag3--Ag4 (Å)	Ag5--Ag6 (Å)
115	20.8687(16)	21.6667(15)	13.9933(11)	91.201(7)	6325.8(8)	1.976	1.972	1.962	2.9769(12)	3.1925(11)	3.0894(11)
160	21.0802(11)	21.664(1)	14.0989(6)	91.074(4)	6437.6(5)	2.168	1.960	1.961	3.1433(9)	3.2087(9)	3.0168(9)
215	21.2199(14)	21.7417(13)	14.3324(9)	90.899(6)	6611.5(7)	2.157	1.992	2.150	3.1293(12)	3.2199(13)	3.0160(12)
255	21.419(2)	21.8985(17)	14.5994(13)	90.728(8)	6847.1(11)	2.144	2.158	2.164	3.121(2)	3.212(2)	3.031(2)
292	21.3259(15)	21.8519(16)	14.6114(9)	90.804(5)	6808.4(8)	2.179	2.160	2.170	3.1265(13)	3.2108(13)	3.0237(13)

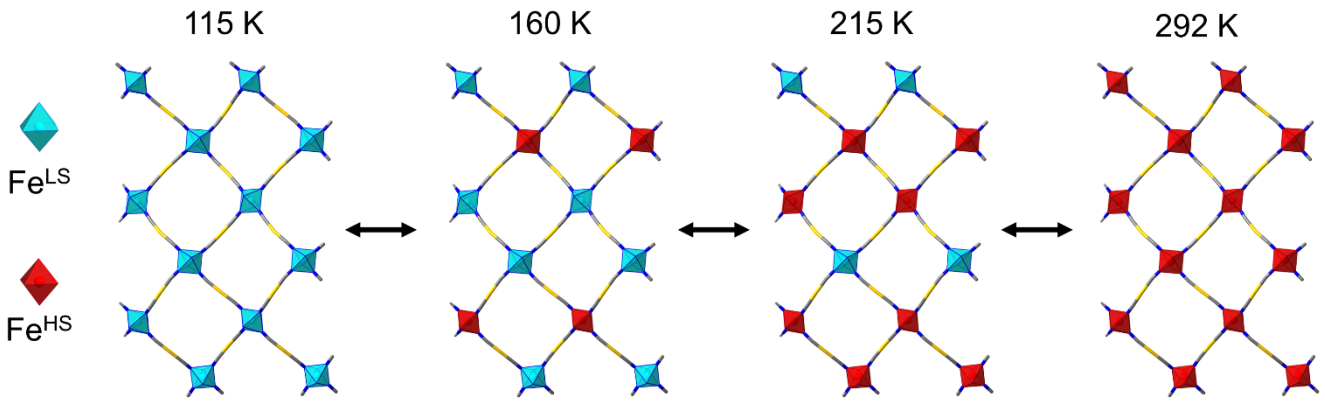

Figure 3. Representation of a single cyanometallic layer of **1** which shows the alteration of LS and HS sites during the SCO process. Crystal structure at 255 K is not shown because of unlocalized spin cites at this temperature.

centers remain in the LS state, while all Fe1 centers transform to the HS state completely. At 160 K, the Fe-N_{CN} bond lengths for Fe1 are 2.13-2.15 Å, and the Fe-N_{pz} lengths are 2.20-2.22 Å. A complete transition of all Fe1 centers corresponds to the spin change of 1/3 of the metal centers, well corroborated by the magnetic susceptibility. The transition of Fe3 centers occurs in the second step. At 215 K, the Fe-N_{CN} bond lengths for Fe3 are 2.12-2.15 Å, and the Fe-N_{pz} lengths are 2.19-2.20 Å. The Fe1 and Fe2 centers remain in the HS and LS states, respectively. These changes correspond to spin transition in 2/3 of the metal centers at 215 K. The Fe2 sites undergo a transformation to the HS state in the third step. The structural features signalize that the spin transition is almost complete: at 255 K the Fe-N_{CN} bond lengths for Fe2 are 2.13-2.14 Å and the Fe-N_{pz} lengths are 2.20-2.21 Å. Interestingly, the equatorial Fe1–N bond lengths at 255 K are slightly shorter then at 160 K, at 255 K Fe-N_{CN} bond lengths are 2.10-2.12 Å, and the Fe-N_{pz} lengths are 2.19-2.20 Å. In the room-temperature (292 K) structure all iron centers are in the HS state. The Fe-N_{CN} bond lengths for Fe1 are 2.15-2.16 Å and the Fe-N_{pz} lengths are 2.21-2.24 Å. The Fe-N_{CN} bond lengths for Fe2 are 2.13-2.15 Å, and the Fe-N_{pz} lengths are 2.20-2.21 Å. The Fe-N_{CN} bond lengths for Fe3 are 2.13-2.16 Å, and the Fe-N_{pz} lengths are 2.23 Å. In the fourth step some crystallographic changes are observed for the coordination environment of Fe1. Fe1-N bond lengths at 292 K increase becoming more HS-like. Additionally, the angle between planes containing Fe1-coordinated pyrazine rings decreases gradually from 52.0° to 44.8° upon heating from 115 to 255 K, while this value increases abruptly to 49.4° at 292 K (Table S1).

In general case, Fe^{II} centers which have less distorted coordination environment, are more likely to undergo HS to LS transition upon cooling.[14a] In case **1** crystallographic measurements were performed in the heating mode and here the same tendency is observed – Fe^{II} centers with higher octahedral distortion parameter are more preferable to transit from the LS state to the HS state upon heating.

Octahedral, trigonal and length distortion parameters for all Fe centers at different temperatures are given in **Table 2**. At 115 K Fe1 has the highest Σ of all iron centers (25.04°) with the major contribution coming from deviation of equatorial N_{CN}–Fe1–N_{CN} angles from 90°. Σ of Fe2 center at this temperature is 10.67°. Notably Σ of Fe3 is 8.79° which in combination with length distortion parameter ζ of 0.097 Å shows that Fe3 center has almost ideal octahedral geometry at 115 K. Fe1 center being the most distorted is the first one to undergo LS→HS transition at heating. Its Σ increases to 28.73° at 160 K. Remarkably, while Fe3 displays an expected increase of Σ up to 11.25° at 160 K, octahedral distortion of Fe2 slightly decreases to 8.92°. Thus, the most distorted LS center at 160 K is Fe3 and it undergoes SCO at the next step of heating with the increase of its octahedral distortion to 15.61° at 215 K. Σ of Fe2 increases just slightly at this step and reaches 10.65° at 215 K. At the third step Fe2 transits to

the HS state and its Σ increases to 11.06° at 255 K. Σ of Fe3 reaches 18.62° at this temperature.

The origin of the 255 K plateau stabilization can be also found upon analysis of octahedral distortions Σ of iron centers. A drastic decrease of Σ from 28.73° to 17.66° is observed for the HS form of Fe1 at heating from 160 to 255 K. This observation indicates that multistability of this system comes also from antiferroelastic interactions between Fe^{II} centers, but not only independent transitions of distinct sites. The short cyanide bridges are very efficient in transferring information concerning the spin state and distortions in cyanometallic layers contribute to the stabilization of intermediate states. In case of **1**, in order for the lattice to adjust to the increase of volume due to LS→HS transition in Fe3 and Fe2, the inverse decrease of $Fe1^{HS}$–N_{CN} bond lengths and Σ is observed at step 3. Such anticooperativity has been previously observed multiple times for similar Hofmann-like systems, exhibiting multistep transitions.[14a-c] Upon further heating Σ of Fe1 increases again and reaches 27.33° at step 4, which is close to the value of Σ for this iron center at 160 K (28.73°) just after the initial LS→HS transition. Octahedral distortion parameters of Fe2 and Fe3 at 292 K are 12.23 and 16.36°, respectively.

At all steps trigonal distortion parameter θ of all iron centers changes in line with Σ, while length distortion parameter ζ of Fe3 displays a gradual increase within the whole heating region. In case of Fe1 and Fe2 ζ slightly deviates in both directions upon heating.

The overall structure of the complex is not affected significantly by the multistep spin transition. The bimetallic cyano-bridged layers form [4,4] networks which create interpenetrated bilayers in the *ac* plane **(Figure 2b,c).** The iron centers are located at the nodes of the network and connected by the $Ag(CN)_2$ bridges. $[Fe\{Ag(CN)_2\}_2]_\infty$ layers are highly puckered because of the presence of bulky substituent at pyrazine ring. The alteration of LS and HS centers in a single cyanometallic layer during the stepped transition is given in **Figure 3**.

The networks communicate through argentophilic interactions with Ag--Ag contacts of 2.9769(12) Å, 3.1925(11) Å, and 3.0894(11)Å (115 K). In the first step of the SCO, the framework geometry changes, and the argentophilic contacts change to 3.1433(9) Å, 3.2087(9) Å and 3.0168(9) Å (160 K). In the following steps, the changes in the framework geometry do not considerably affect these metal-to-metal contacts (**Table 1**). There are no other notable weak interactions in the structure. Moreover, to the best of our knowledge, **1** is the first example of a guest-free Hofmann clathrate analogue which exhibits a four-step transition. This complex shows that the presence of a set of antagonistic host-guest interactions is not a necessary requirement for the occurrence of multistep transitions, while the introduction of a ligand with a bulky substituent can generate different SCO-active sites.

The evolution of the crystal structures can be analyzed as well from the change of unit cell parameters that were determined by single-crystal XRD at different temperatures during heating between 115 and 280 K (**Figure 4**). This confirms that the step character is associated with a phase transformation of an individual compound and is not due to phase mixing. Each step of the spin transition is accompanied by a significant change in the lattice dimensions. While the *b*-parameter gradually increases from 115 to 280 K by approx. 1%, the *a* and *c* parameters are affected considerably in each step of the SCO. The overall changes are Δ*a* = 2.5%, Δ*c* = 4.6% and ΔV = 8.5%.

Table 2. Octahedral Σ, trigonal θ and length ζ distortion parameters of all Fe centres at different temperatures.

		115 K	160 K	215 K	255 K	292 K
Fe1	Σ (°)[a]	25.04	28.73	23.97	17.66	27.33
	θ (°)[b]	68.64	80.39	67.08	51.23	71.96
	ζ (Å)[c]	0.131	0.170	0.186	0.229	0.179
Fe2	Σ (°)	10.67	8.92	10.65	11.06	12.23
	θ (°)	33.39	28.19	34.86	35.60	39.63
	ζ (Å)	0.127	0.157	0.133	0.188	0.191
Fe3	Σ (°)	8.79	11.25	15.61	18.62	16.36
	θ (°)	28.64	36.72	44.96	56.06	55.35
	ζ (Å)	0.097	0.126	0.177	0.193	0.231

[a] $\Sigma = \Sigma_{i=1}^{12}|90° - \alpha_i|$, [b] $\Theta = \Sigma_{i=1}^{24}|60° - \beta_i|$, [c] $\zeta = \Sigma_{i=1}^{6}|(Fe–N_i)-<Fe–N>|$, where α are 12 cis-N–Fe–N angles, β are 24 unique torsion angles between the adjacent N atoms on opposite triangular faces viewed along the pseudo-threefold axes.

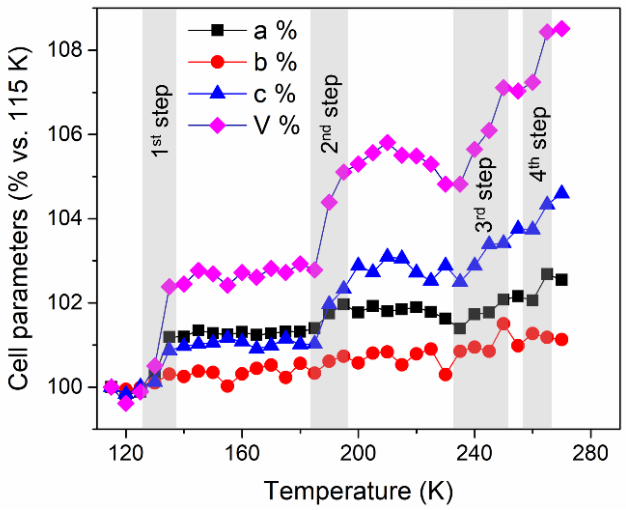

Figure 4. Cell parameters of **1** (vs. LS form at 115 K) as a function of temperature. The *a*, *c* and V parameters change stepwise with four steps resolved, while the *b* parameter changes gradually within 115-280 K range (5 K interval).

The transition temperatures determined by XRD analysis match the transitions temperatures found from the magnetic susceptibility data. SCO curve obtained from single-crystal XRD experiment superimposes well with the curve obtained in magnetic measurements (**Figure S2**) showing a good agreement between SCO properties of a single crystal and a polycrystalline powder sample.

The first step occurs at $T_c(1)$ = 132 K, the second step at $T_c(2)$ = 189 K, and the fourth step occurs at $T_c(4)$ = 263 K. The transition temperature of the third step is difficult to determine. First, the cell volume shrinks upon heating from 220 to 230 K by 0.7%, and it increases upon heating from 230 to 255 K by 2.2%. We were unable to structurally trace the origin of these small alterations

Table 3. Mössbauer hyperfine parameters of **1** at different temperatures. Isomer shift (δ), quadrupole splitting (ΔE_Q), linewidth (w) and a form content are provided.

	LS				HS			
T (K)	δ (mm s^{-1})	ΔE_Q (mm s^{-1})	w (mm s^{-1})	Content (%)[b]	δ (mm s^{-1})	ΔE_Q (mm s^{-1})	w (mm s^{-1})	Content (%)[b]
100	0.4635(21)	0.293(15)	0.1425(98)	100	--	--	--	0
160	0.4632(61)	0.277(55)	0.145(44)	67(2)	1.095(12)	1.699(25)	0.140(13)	33(1)
215	0.422(23)	0.255(55)	0.153(36)	36(2)	1.137(24)	1.295(49)	0.1753(100)	64(2)
255	0.4[a]	0.2[a]	0.15[a]	13(3)	1.1165(75)	1.206(15)	0.1982(81)	87(4)
293	--	--	--	0	1.0679(21)	1.1246(42)	0.1370(34)	100

[a] Parameters were fixed during the fit. [b] Provided content values correspond to the total spin fractions at each temperature.

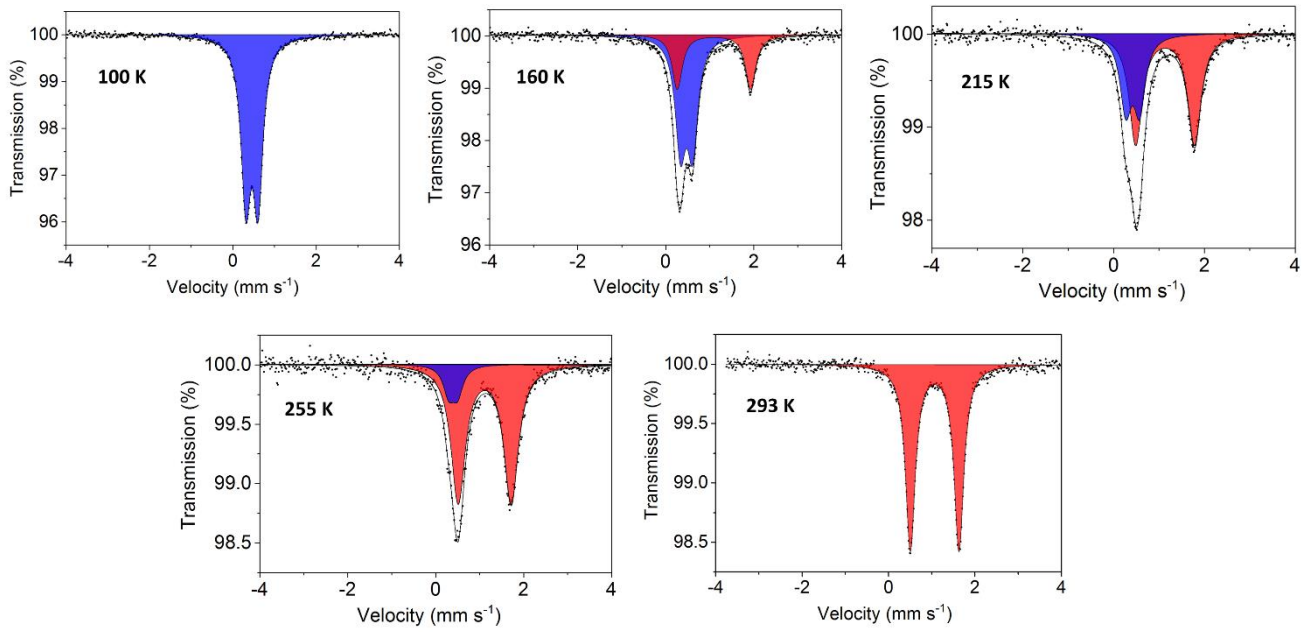

Figure 5. Mössbauer spectra of **1** at different temperatures (100, 160, 215, 255 and 293 K). LS doublets are shown in blue and HS doublets are shown in red. A complete LS to HS transition occurs upon heating from 100 K to 293 K.

over a narrow temperature range. It is assumed that this decrease in the unit cell size should be related to the re-distribution of LS-HS character between two Fe sites: the spin state at Fe3 becomes more HS-type, while that at Fe1 becomes more LS-like. This may also be the reason why we observe a four-step transition upon heating and a three-step transition upon cooling. One can suppose a direct HS to LS transformation of Fe2 crystallographic center at the first step of cooling, namely without formation of any intermediate spin mixed crystallographic centers and more densely packed structures (like at c.a. 230 K upon heating).

The spin fractions at each step were characterized by Mössbauer spectroscopy. Mössbauer spectra of **1** are shown in **Figure 5**, the corresponding hyperfine parameters are summarized in **Table 3**. They show a complete SCO between a LS form (100 K) and a HS form (293 K).

In this experiment sample of **1** was immersed into the cryostat at liquid nitrogen temperature and all subsequent measurements were performed in heating mode. The spectrum at 100 K reveals only one LS-doublet with an isomer shift of 0.4635(21) mm s^{-1} and a quadrupole splitting of 0.293(15) mm s^{-1}. It is worth noting the absence of any residual HS fractions at 100 K, means no centers were quenched in HS state in this experiment. The spectra at 160 and 215 K show a co-existence of LS and HS centers in ratios of 2:1 and 1:2. This is in harmony with the magnetic and structural data. The spectrum at 255 K reveals that 23% of the Fe centers have transformed to the HS state in the third step. The value of 26% extracted from the susceptibility measurements is very close to that obtained from Mössbauer spectroscopy. The room temperature spectrum (293 K) shows only one HS doublet with an isomer shift of 1.068(2) mm s^{-1} and a quadrupole splitting of 1.125(4) mm s^{-1}. The remaining 13% of the LS centers transform to the HS state in step 4 (8% based on the susceptibility measurements).

There are some previous examples of four-step transitions in cyanometallic complexes with bridging pyridine-based ligands and $\{Ag(CN)_2\}^-$ [14b,d,f,g] and $\{Au(CN)_2\}^-$ [12a,14d] units. It should be

noted that such multistep transformations are also possible in tetracyanometallic analogues. A four-step spin transition was previously observed in Fe-based complex with a Schiff-base triazolic ligand[14a] supported by tetracyanoplatinate as co-ligand.

Conclusion

In summary, we have synthesized and analyzed a new cyano-bridged bimetallic framework compound with a four-step spin transition, which is accompanied by a stepwise transformation of the crystal structure. The lattice symmetry is maintained through the cascade of phase transitions.
Three crystallographic non-equivalent sites of iron favor the step-character of the transition, while the stabilization of five different spin phases may be explained by minor packing effects.

Experimental Section

Synthesis. The title complex was prepared by mixing iron tosylate $Fe(OTs)_2 \cdot 6H_2O$ (50.6 mg, 0.1 mmol) and 2-ethoxypyrazine (24.8 mg, 0.2 mmol) in ethanol (1 ml) and potassium dicyanoargentate (39.8 mg, 0.2 mmol) in water (1 ml). The yellow precipitate was removed by centrifugation, washed with water and dried in air. Single crystals of the title complex were obtained by the slow diffusion method: $KAg(CN)_2$ in water (1 ml) and $Fe(OTs)_2$ with ethoxypyrazine in methanol (1 ml) were allowed to diffuse through a layer of water-methanol (2:1, 2 ml) over a period 2 weeks. Elemental analysis for $C_{16}H_{16}Ag_2FeN_8O_2$: calc. C, 30.80; H, 2.58; N, 17.96; found C, 30.94; H, 2.66; N, 17.57. IR spectrum of **1** is given in **Figure S3**.

Magnetic measurements. Temperature dependent magnetic susceptibility measurements were carried out with a Quantum-Design MPMS-XL-5 SQUID magnetometer equipped with a 5 T magnet in the 70–290 K temperature range with a cooling/heating rate of 1 K min^{-1}, with a magnetic field of 0.5 T. Diamagnetic corrections derived from Pascal constants were applied.

Mössbauer measurements. ^{57}Fe Mössbauer spectra were recorded with a ^{57}Co source embedded in a rhodium matrix using a conventional constant-acceleration Mössbauer spectrometer equipped with a liquid-nitrogen cryostat. The absorber was prepared by placing 50 mg of the powdered sample in a PMMA holder. Fits of the experimental data were performed with Recoil software.[17a] Hyperfine parameters uncertainties given in parentheses were evaluated using the covariance matrix of the fit. Isomer shifts are given relatively to iron metal at ambient temperature.

Powder XRD. The PXRD patterns were acquired on Shimadzu XRD-6000 diffractometer using Cu-Kα radiation (5–50° range, 0.05° step).

Single crystal XRD. A crystal of 1 was mounted in a crystal holder and placed in a stream of nitrogen at 115 K. For further measurements the crystal was heated and thermalized at different temperatures. X-ray diffraction data were collected by using an Oxford-Diffraction XCALIBURE CCD diffractometer with graphite-monochromated Mo-Kα radiation. The unit cell determination and data integration were carried out using the CrysAlisPro package from Oxford Diffraction.[17b] Multi-scan correction for absorption was applied. All structures were solved using intrinsic phasing methods and refined by full-matrix least-squares on F2 using SHELXT and SHELXL[17c] and the graphical user interface Olex2.[17d] Non-hydrogen atoms were refined with anisotropic thermal parameters. Aromatic hydrogen atoms were placed at calculated positions and refined using a riding model. Octahedral, trigonal and length distortion parameters were calculated using OctaDist software.[17d] Deposition Numbers <url href="https://www.ccdc.cam.ac.uk/services/structures?id=doi:10.1002/chem.202200924"> 1901733 (for 160 K), 1901734 (for 292 K), 1901735 (for 215 K), 1901736 (for 115 K), 1901737 (for 255 K)</url> contain(s) the supplementary crystallographic data for this paper. These data are provided free of charge by the joint Cambridge Crystallographic Data Centre and Fachinformationszentrum Karlsruhe <url href=" http://www.ccdc.cam.ac.uk/structures ">Access Structures service</url>.

Acknowledgements

Authors acknowledge the financial support from the Ministry of Education and Science of Ukraine (grant 22BF037-09) and the courage of the Armed Forces of Ukraine that made the submission of this manuscript possible.

Keywords: spin crossover • Hofmann clathrates analogues • multistep transitions • iron(II) • substituted pyrazine

[1] M. Wuttig, N. Yamada, *Nat. Mater.* **2007**, *6*, 824–832.
[2] A. Miriyev, K. Stack, H. Lipson, *Nat. Commun.* **2017**, *8*, 596.
[3] G. Mattoni, P. Zubko, F. Maccherozzi, A. J. H. van der Torren, D. B. Boltje, M. Hadjimichael, N. Manca, S. Catalano, M. Gibert, Y. Liu, J. Aarts, J.-M. Triscone, S. S. Dhesi, A. D. Caviglia, *Nat. Commun.* **2016**, *7*, 13141.
[4] a) K. S. Murray, in *Spin-Crossover Materials* (Ed.: M.A. Halcrow), John Wiley & Sons Ltd, Oxford, **2013**, pp. 1–54; b) P. Gütlich, H. A. Goodwin, in *Spin Crossover Transition Metal Compounds I* (Eds.: P. Gütlich, H.A. Goodwin), Springer, Berlin, Heidelberg, **2004**, pp. 1–47.
[5] a) V. Jornet-Mollá, Y. Duan, C. Giménez-Saiz, Y.-Y. Tang, P.-F. Li, F. M. Romero, R.-G. Xiong, *Angew. Chem. Int. Ed.* **2017**, *56*, 14052–14056; *Angew. Chem.* **2017**, *129*, 14240-14244; b) K. Senthil Kumar, I. Šalitroš, Z. Boubegtiten-Fezoua, S. Moldovan, P. Hellwig, M. Ruben, *Dalton Trans.* **2018**, *47*, 35–40.
[6] a) H. J. Shepherd, I. A. Gural'skiy, C. M. Quintero, S. Tricard, L. Salmon, G. Molnár, A. Bousseksou, *Nat. Commun.* **2013**, *4*, 2607; b) M. D. Manrique-Juárez, S. Rat, L. Salmon, G. Molnár, C. M. Quintero, L. Nicu, H. J. Shepherd, A. Bousseksou, *Coord. Chem. Rev.* **2016**, *308*, 395–408.
[7] a) M. Ohba, K. Yoneda, G. Agustí, M. Carmen Muñoz, A. B. Gaspar, J. A. Real, M. Yamasaki, H. Ando, Y. Nakao, S. Sakaki, S. Kitagawa, *Angew. Chem. Int. Ed.* **2009**, *48*, 4767–4771; *Angew. Chem.* **2009**, *121*, 4861-4865; b) X. Bao, H. J. Shepherd, L. Salmon, G. Molnár, M.-L. Tong, A. Bousseksou, *Angew. Chem. Int. Ed.* **2013**, *52*, 1198–1202; *Angew. Chem.* **2013**, *125*, 1236-1240.
[8] K. A. Hofmann, F. Höchtlen, *Ber. Dtsch. Chem. Ges.* **1903**, *36*, 1149–1151.
[9] T. Kitazawa, Y. Gomi, M. Takahashi, M. Takeda, M. Enomoto, A. Miyazaki, T. Enoki, *J. Mater. Chem.* **1996**, *6*, 119–121.
[10] a) V. Niel, J. M. Martinez-Agudo, M. Carmen Muñoz, A. B. Gaspar, J. A. Real, *Inorg. Chem.* **2001**, *40*, 3838–3839; b) A. Galet, M. Carmen Muñoz, V. Martínez, J. A. Real, *Chem. Commun.* **2004**, *10*, 2268–2269; c) S. Bonhommeau, G. Molnár, A. Galet, A. Zwick, J.-A. Real, J. J. McGarvey, A. Bousseksou, *Angew. Chem. Int. Ed.* **2005**, *44*, 4069–4073; *Angew. Chem.* **2005**, *117*, 4137-4141; d) R. Ohtani, K. Yoneda, S. Furukawa, N. Horike, S. Kitagawa, A. B. Gaspar, M. C. Muñoz, J. A. Real, M. Ohba, *J. Am. Chem. Soc.* **2011**, *133*, 8600–8605; e) L. Piñeiro-López, M. Seredyuk, M. C. Muñoz, J. A. Real, *Chem. Commun.* **2014**, *50*, 1833–1835; f) O. I. Kucheriv, I. O. Fritsky, I. A. Gural'skiy, *Inorganica Chim. Acta* **2021**, *521*, 120303.
[11] M. Carmen Muñoz, J. A. Real, *Coord. Chem. Rev.* **2011**, *255*, 2068–2093; a) I. A. Gural'skiy, B. O. Golub, S. I. Shylin, V. Ksenofontov, H. J. Shepherd, P. R. Raithby, W. Tremel, I. O. Fritsky, *Eur. J. Inorg. Chem.* **2016**, *2016*, 3191–3195; b) I. A. Gural'skiy, S. I. Shylin, B. O. Golub, V. Ksenofontov, I. O. Fritsky, W. Tremel, *New J. Chem.* **2016**, *40*, 9012–9016.
[12] a) J. E. Clements, J. R. Price, S. M. Neville, C. J. Kepert, *Angew. Chem. Int. Ed.* **2016**, *55*, 15105-15109; *Angew. Chem.* **2016**, *128*, 15329–15333; b) N. F. Sciortino, K. R. Scherl-Gruenwald, G. Chastanet, G. J. Halder, K. W. Chapman, J.-F. Létard, C. J. Kepert, *Angew. Chem. Int. Ed.* **2012**, *51*, 10154–10158; *Angew. Chem.* **2012**, *124*, 10301-10305.

[13] J. Cruddas, B. J. Powell, *Inorg. Chem. Front.* **2020**, *7*, 4424–4437.

[14] a) N. F. Sciortino, K. A. Zenere, M. E. Corrigan, G. J. Halder, G. Chastanet, J.-F. Létard, C. J. Kepert, S. M. Neville, *Chem. Sci.* **2017**, *8*, 701–707; b) C.-J. Zhang, K.-T. Lian, G.-Z. Huang, S. Bala, Z.-P. Ni, M.-L. Tong, *Chem. Commun.* **2019**, *55*, 11033–11036; c) A. T. Brennan, K. A. Zenere, C. J. Kepert, J. K. Clegg, S. M. Neville, *Inorg. Chem.* **2021**, *60*, 3871–3878; d) F. J. Valverde-Muñoz, C. Bartual-Murgui, L. Piñeiro-López, M. C. Muñoz, J. A. Real, *Inorg. Chem.* **2019**, *58*, 10038–10046; e) W. Liu, Y.-Y. Peng, S.-G. Wu, Y.-C. Chen, M. N. Hoque, Z.-P. Ni, X.-M. Chen, M.-L. Tong, *Angew. Chem. Int. Ed.* **2017**, *56*, 14982-14986; *Angew. Chem.* **2017**, *129*, 15178–15182; f) C.-J. Zhang, K.-T. Lian, S.-G. Wu, Y. Liu, G.-Z. Huang, Z.-P. Ni, M.-L. Tong, *Inorg. Chem. Front.* **2020**, *7*, 911–917; g) S. Wu, S. Bala, Z. Ruan, G. Huang, Z. Ni, M. Tong, *Chinese Chem. Lett.* **2021**, 8–11.

[15] Y.-Y. Peng, S.-G. Wu, Y.-C. Chen, W. Liu, G.-Z. Huang, Z.-P. Ni, M.-L. Tong, *Inorg. Chem. Front.* **2020**, *7*, 1685–1690.

[16] a) O. I. Kucheriv, S. I. Shylin, V. Ksenofontov, S. Dechert, M. Haukka, I. O. Fritsky, I. A. Gural'skiy, *Inorg. Chem.* **2016**, *55*, 4906–4914; b) S. I. Shylin, O. I. Kucheriv, S. Shova, V. Ksenofontov, W. Tremel, I. A. Gural'skiy, *Inorg. Chem.* **2020**, *59*, 6541–6549.

[17] a) K. Lagarec, D. G. Rancourt, *Nucl. Instrum. Methods Phys. Res. Sect. B Beam Interact. with Mater. Atoms* **1997**, *129*, 266–280; b) CrysAlisPro, *Version 1.171.39.46, Rigaku Oxford Diffraction, Yarnton, UK* **2018**; c) G. M. Sheldrick, *Acta Crystallogr. Sect. C Struct. Chem.* **2015**, *71*, 3–8; d) O. V. Dolomanov, L. J. Bourhis, R. J. Gildea, J. A. K. Howard, H. Puschmann, J. Appl. Crystallogr. 2009, 42, 339–341; e) R. Ketkaew, Y. Tantirungrotechai, P. Harding, G. Chastanet, P. Guionneau, M. Marchivie, D. J. Harding, *Dalton Trans.* **2021**, *50*, 1086–1096.

Entry for the Table of Contents

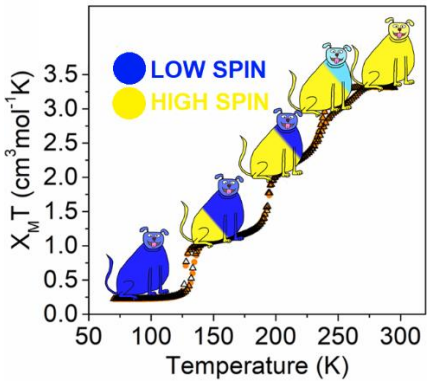

Here we report on a new guest-free Hofmann clathrate analogue Fe(2-ethoxypyrazine)$_2${Ag(CN)$_2$}$_2$ which undergoes a four-step spin crossover during the transition from the low-spin to the high-spin state. At the first step 1/3 of centers become high spin, at the second step another 1/3 of centres become high spin, at the third step spin mixed crystallographic centres are observed, and after the fourth step all centers are high spin.